Autonomous reconfigurable hybrid tail-sitter UAV U-Lion

Kangli WANG*, Yijie KE & Ben M. CHEN

Unmanned Systems Research Group, 4 Engineering Drive 3, National University of Singapore, Singapore 117583, Singapore

Abstract   We present in this work the development of a novel hybrid unmanned aircraft platform, U-Lion, which has both vertical take-off and landing (VTOL) and cruising flight capabilities. Our design is in tail-sitter structure with reconfigurable wings, which combines the advantages of a fixed-wing plane and a rotor helicopter effectively. This allows it to transit from vertical take-off to hovering, before flying in cruise mode for efficient long duration flight. The propulsion comes from two coaxial contra-rotating motors fixed on a gimbal mechanism, which can change the direction of the motors for the required thrust. This thrust-vectored propulsion system primarily provides control in the VTOL mode but also enhances flight capabilities in the cruise mode. The hybrid aircraft is equipped with GPS and airspeed sensors, and has an onboard avionic system with advanced flight control algorithms to perform fully autonomous VTOL and cruising flights, in addition to transiting effectively between VTOL and cruising flight modes. The overall design has been successfully verified by actual flight experiments.

Keywords   unmanned aerial vehicle, vertical take-off and landing, hybrid platform, aircraft platform design, flight control system

1   Introduction

The development of hybrid unmanned aerial vehicles (UAVs) has attracted great interest from both academia and industry. Hybrid UAVs with VTOL and fixed-wing cruise operating modes have potential applications in military and civilian operations, especially where there are severe constraints in their operating environment. The VTOL capability minimizes the dependency of the take-off and landing facilities and cruise flying capability allows hybrid UAVs to perform long range and duration tasks.

Two typical hybrid UAV models, the quad-plane type and the tail-sitter type, are intensively studied and reported in the open literature. The quad-plane type achieves the hybrid capability by installing multiple rotors to a fixed-wing airplane. Thus, it can take off and land vertically like the usual multi-rotor aircraft and can perform cruising flight like a fixed-wing plane. However, its two separate propulsion systems result in less weight efficiency. On the other hand, the tail-sitter UAVs utilize only a single

---

* Corresponding author (email: wangkangli@u.nus.edu)

propulsion structure. It can perform more rapid transition between the VTOL and cruise modes. The transition process is, however, more difficult to automate due to a large change in the angle of attack (AOA) during the process.

Many work have been done in designing both types of unconventional platforms and in studying algorithms for stable and robust transition flights for tail-sitter UAVs (see, for example, Refs. [1, 2] and the references therein). For the hybrid UAV proposed in [2], its novelty lies in the usage of four rotors, such that the UAV can fly in cruise mode without control surfaces. However, during high speed of cruise flight, the titling torques provided by differential thrust from the rotors are not as effective as control surfaces. As a result, the agility in cruise flight is limited. In [1], a delta wing configuration tail-sitter UAV is proposed. The platform is simple in configuration with only two rotors and two control surfaces. However, the titling torque of the UAV in VTOL or transition is provided by the deflection of control surfaces within the propeller slipstream. The control input may be not effective under wind disturbance.

In this work, we propose to develop an autonomous hybrid UAV, U-Lion, which not only has two flight modes, but is also capable of restructuring the platform shape by sweeping its wings. This special design aims to achieve stable and efficient flight in both modes. The gimbal ring based vectored thrust mechanism provides the propulsion for both flying modes and sufficient controllability for transition as well. A tail with multiple control surfaces is implemented to increase control actuators for more stable flight and agile maneuverability. A flight control system is developed and implemented to effectively control the attitude and the position of the aircraft fully autonomously. The overall design of the hardware platform and the flight control system are fully tested by actual flight experiments. Readers are encouraged to view the flight video accompanying this manuscript for more information.

The outline of the remaining manuscript is as follows: We present in Section 2 a brief introduction to the platform design of U-Lion. Sections 3 and 4 present the inner loop and outer loop flight control framework, respectively. We then show in Section 5 experimental flight test data and results. Finally, we draw some concluding remarks in Section 6.

2 Platform design and its key features

U-Lion was designed in tail-sitter configuration with reconfigurable wings to enhance the flying performance for both modes. With the same design methodology as presented in our previous work [3], we continue to optimize U-Lion platform. The first prototype of U-Lion (presented in [3]) and current prototype are shown in Figure 1. The computer-aided design (CAD) for current prototype is shown in Figure 2. In the following text, 'U-Lion' without further specification refers to the current prototype. The improvements of the design are listed as follows:

Optimized layout. Swept-wing tail-sitter configuration was optimized to balance between aerodynamics and weight. Wings are able to be fully folded as shown in Figure 1(b), which facilitates the storage and transportation of the UAV. To our knowledge, there is no similar platform in the literature with such capability.

Compact structure. Carbon fiber and industrial plastic materials formed the aircraft structure. Strength verification was conducted for whole platform via software simulations, and weight minimization was conducted through several iterations.

Aerodynamics efficiency design. Besides the wings, a foam fuselage was designed to increase aerodynamic efficiency. The fuselage can provide additional lift force, while serving as the house for internal electronics. The fuselage was specifically designed for low Reynolds number aerodynamics environment [4], thus it has a higher efficiency than common airfoil-shaped design.

The three main design features of U-Lion are listed as follows:

1. Vectored thrust. The propulsion motors of U-Lion are the Himax CR3516 coaxial contra-rotating motors. The maximum thrust provided by the motors is approximately 30 N powered by one 3-cell lithium polymer battery, which provides the platform a thrust to weight ratio of approximately 1.7. The motors are fixed on two gimbal rings similar to the design shown in Figure 1(a). The gimbal rings can

Figure 1 (Color online) Two prototypes for U-Lion. (a) U-Lion first prototype; (b) U-Lion current prototype.

change the direction of the thrust through the servo movements. The gimbal servos are Hitec HS85MG servos with maximum rotating speed of 6.5 rad/s which is sufficiently fast for U-Lion. The vectored thrust controls the six degrees of motion in VTOL mode and also provides additional control inputs in cruise mode. The maximum tilting angle of the vectored thrust in pitch direction is 30°. The direct drive vectored thrust propulsion system releases the dependency on the input airflow which is required by the control surface based actuators. As a result, the control performance of U-Lion is more robust in VTOL mode and transition process under wind disturbance.

2. Reconfigurable wings. The reconfigurable-wing design enables U-Lion to adapt to different flying modes more effectively. The reconfigurable function is triggered by a four-bar mechanism same as previous prototype as shown in Figure 1(a). In VTOL mode, the wings are folded to reduce the effect of wind gust, and the folded wings can also serve to guide the propeller slipstream to tail fins, which can increase the effectiveness of the tail-fin control. Folding the wings also reduces the moment of inertia in yawing direction which results in larger yawing controllability. In cruise mode, the wings are fully swept forward to provide the lift force.

3. Multiple control-surfaces tail. The previous prototype designed a carbon tube cross shape structure as landing skid. While for current prototype, the tail structure also serves as the landing skid for U-Lion. The tail for current prototype is a cross shape structure made of carbon fiber plates as shown in Figure 1(b). The control surfaces on the tail provide extra control inputs in VTOL mode and act as pitching and yawing control actuators in cruise mode.

Furthermore, low density materials were chosen so that the weight of U-Lion is minimized. The main frame of U-Lion is made of carbon fiber tubes and plates. The tail control surfaces are made of balsa wood. The total weight of U-Lion is reduced from 2.2 kg (first prototype) to 1.77 kg (current prototype). The aerodynamic lift in cruise mode is mainly generated from the wings and fuselage. The focus of wing design is on maximizing the aspect ratio and wing area under the constraints of total weight and the ability of full wing retraction. For simplicity, the foam wings from a model glider aircraft (Multiplex Easystar 2) with airfoil shape NACA2411 are utilized with the wingtips removed. The total wing area is 0.208 m^2 and the aspect ratio of the wings is 6.78. The fuselage was designed with the aim to increase aerodynamic lift but maintaining a minimal weight. Low Reynolds number airfoils SA8037 and NACA0015 were used

(a) (b)
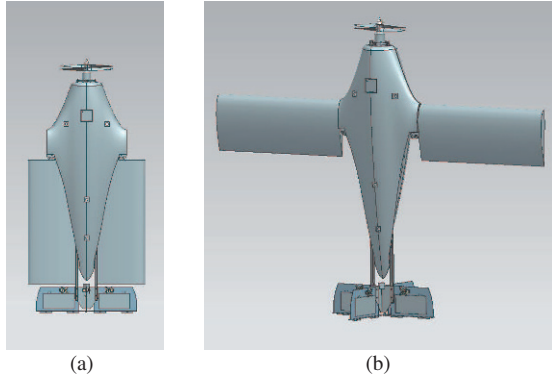
Figure 2 (Color online) CAD design of U-Lion. (a) U-Lion wing close CAD view; (b) U-Lion wing open CAD view.
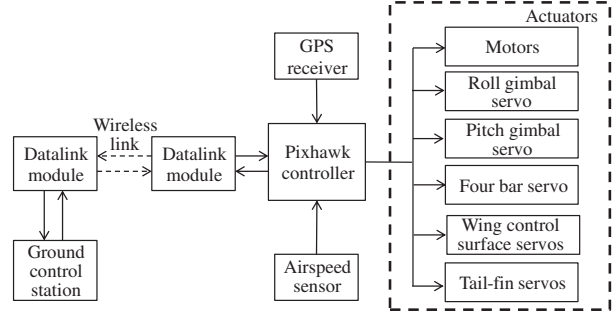
Figure 3 Avionics system.

Table 1 The specifications of U-Lion

Weight	1.77 kg	Flight endurance (VTOL)	7 min
Max thrust	30 N	Flight endurance (Cruise)	12 min
Nominal cruise speed	15 m/s	Dimensions (wings open)	1.37 m × 1.07 m × 0.4 m
Nominal cruise angle of attack	10°	Dimensions (wings close)	0.46 m × 1.07 m × 0.4 m
Maximum cruise speed	40 m/s		

to construct the fuselage body [4,5], and EPO foam was chosen as the material of the fuselage body. The final fuselage weighs 197 g.

In current U-Lion prototype, an avionics system that enables U-Lion with fully autonomous capability was implemented. The avionics system overview is shown in Figure 3. The flight control system was developed based on the open source Pixhawk autopilot system [6]. An Ublox M8N global positioning system (GPS) sensor and a 3DR digital airspeed sensor were connected to the Pixhawk controller to provide accurate position and airspeed measurements. The onboard flight controller communicates with the ground control station (GCS) through a 3DR Radio Telemetry datalink module. The gimbal rings and control surfaces are actuated by servos through pulse width modulation (PWM) signals generated by the flight controller. The specification of U-Lion is shown in Table 1.

3 Inner loop control system design

The inner loop control in this manuscript refers to the attitude control for tracking the desired attitude reference. The attitude estimation is provided by the Pixhawk autopilot attitude and heading reference system (AHRS). The Pixhawk autopilot system incorporates a 3-axis gyro, an accelerometer, a magnetometer and a micro-controller as its main processor. An extended Kalman filter (EKF) is run onboard to estimate the attitude of the aircraft. On top of that, a complementary filter is applied to obtain the position and velocity estimation of the UAV with the aid of the GPS sensor.

We propose to assign two different body coordinate frames for U-Lion, one in the VTOL mode, the other in the cruise mode, as shown in Figure 4. With these two frames, we are able to follow a similar approach as in [7] to obtain the Euler angle representation for each mode without having singularity issues. It simplifies the flight control system design and it is intuitive for monitoring by ground operators. There are three flying modes adopted as shown in Figure 5, i.e., the VTOL mode, the cruising mode, and the transition mode. The attitude control associated with the VTOL mode and transition mode is designed by directly utilizing the rotation matrix while that for the cruise flying mode is based on the usual Euler angle representation for simplicity.

In this manuscript, we adopt the following notations for coordinate rotations: The rotation matrix expressing the transformation from Frame $\boldsymbol{F}_a$ to Frame $\boldsymbol{F}_b$ is represented as $\boldsymbol{R}_{b/a}$. The $\boldsymbol{X}$-axis of Frame
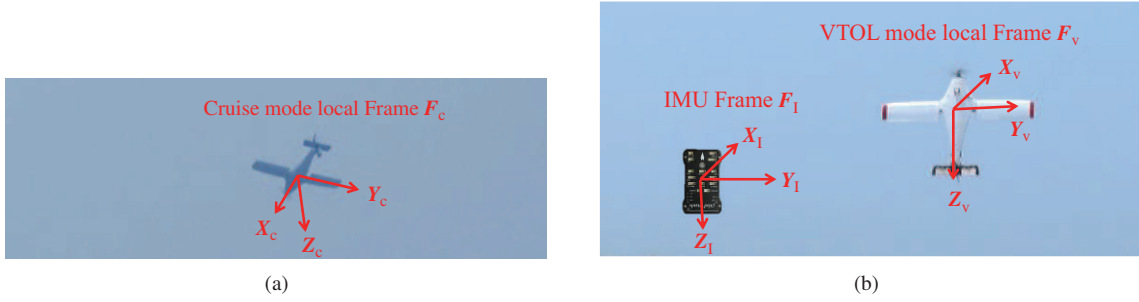
Figure 4 (Color online) The two local frames proposed. (a) U-Lion cruise flying frame; (b) U-Lion VTOL flying frame.

F_a expressed in the local NED frame is denoted as X_a, whereas the X-axis of Frame F_a expressed in Frame F_b is denoted as X_a^b. In the following text, the coordinate vectors or rotations related to the VTOL frame are denoted with a letter 'v', those related to cruise frame are denoted with a letter 'c' and those related to the local NED frame are denoted with a letter 'n'. The rotation about an axis K with an angle γ is denoted as $R(K, \gamma)$.

3.1 VTOL mode

Given a reference rotation matrix, R_r, an rotation angle generator (RAG) will calculate the angles of rotation around the body frame axes to match the reference as depicted in Figure 6. The RAG will first align the Z_v-axis of U-Lion with the reference Z_r-axis in the shortest path, and then to rotate about the newly obtained Z_v-axis to match the heading reference [8–10]. Once the Z_v-axis is superimposed with Z_r-axis, the force will point to the desired direction and the desired motion could be achieved even if the heading is not well matched. This is critical for the control of U-Lion because its rolling/pitching dynamics are much faster than its yawing dynamics. The gimbal ring based vectored thrust can provide more control authority in roll/pitch channels to achieve faster position response.

As shown in Figure 6, the frame in blue is the body frame of U-Lion in the VTOL mode, F_v. The reference frame is shown in solid red, denoted as Frame F_r. The intermediate frame after aligning Z_v-axis with Z_r-axis is represented by the dashed red frame, denoted as Frame F_{int}. In the first step of the RAG, Z_v-axis is aligned with Z_r-axis by rotating around K-axis by an angle of γ, where K-axis is perpendicular to the two Z axes,

$$K = \frac{Z_v \times Z_r}{||Z_v \times Z_r||}, \quad \gamma = \text{atan2}(||Z_v \times Z_r||, Z_v Z_r).$$

This K-axis can be obtained in the VTOL frame by $K^v = R_{v/n} K$, where $R_{v/n} = R_{n/v}^T$ and $R_{n/v}$ is obtained by the onboard EKF algorithm. Let $K^v = (k_x, k_y, k_z)^T$, the rotation about K^v-axis with angle γ is

$$R_{int/v} = R(K^v, \gamma) = \begin{pmatrix} k_x k_x v_\gamma + c_\gamma & k_x k_y v_\gamma - k_z s_\gamma & k_z k_x v_\gamma + k_y s_\gamma \\ k_x k_y v_\gamma + k_z s_\gamma & k_y k_y v_\gamma + c_\gamma & k_z k_y v_\gamma - k_x s_\gamma \\ k_x k_z v_\gamma - k_y s_\gamma & k_y k_z v_\gamma + k_x s_\gamma & k_z k_z v_\gamma + c_\gamma \end{pmatrix},$$

where $s_\gamma = \sin(\gamma)$, $c_\gamma = \cos(\gamma)$ and $v_\gamma = 1 - \cos(\gamma)$. It follows from the expression of K^v that $k_z = 0$. Then for small rotation $\Delta\gamma$ about K^v-axis, we have

$$R(K^v, \Delta\gamma) = \begin{bmatrix} 1 & 0 & k_y \Delta\gamma \\ 0 & 1 & -k_x \Delta\gamma \\ -k_y \Delta\gamma & k_x \Delta\gamma & 1 \end{bmatrix}. \tag{1}$$
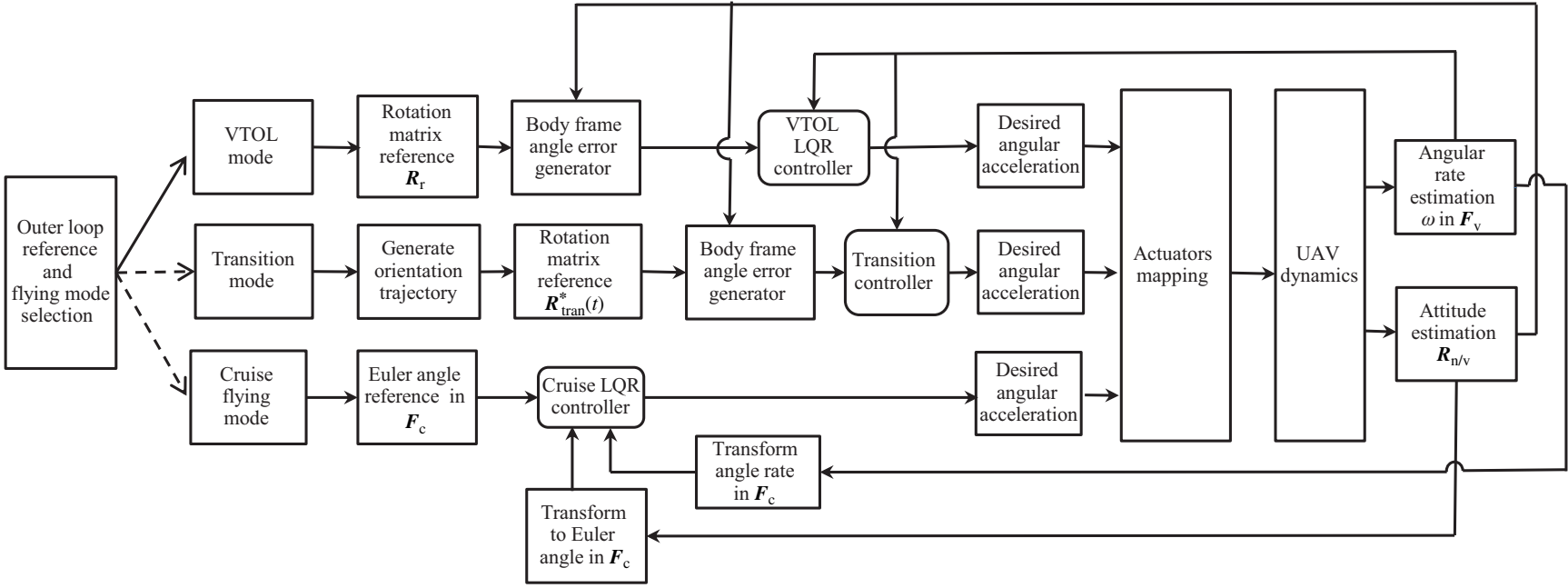
Figure 5   The inner loop control structure.

(a)   (b)   (c)
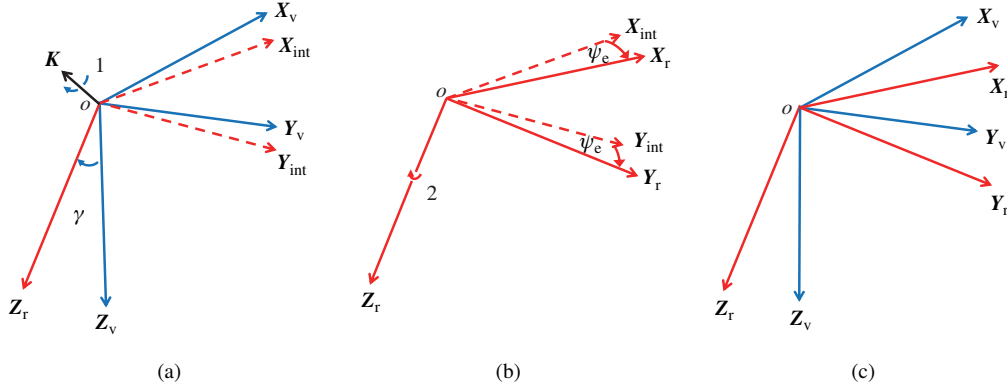
Figure 6 (Color online) The body frame rotation angle generating logic. (a) Align $\boldsymbol{Z}_{\mathrm{v}}$-axis with the $\boldsymbol{Z}_{\mathrm{r}}$-axis by rotating about the $\boldsymbol{K}$-axis which is perpendicular to the two axes by an angle of γ and results in an intermediate frame $\boldsymbol{F}_{\mathrm{int}}$; (b) rotate the frame $\boldsymbol{F}_{\mathrm{int}}$ about $\boldsymbol{Z}_{\mathrm{r}}$-axis by an angle of ψ_{e} to reach the reference axis; (c) the original frame $\boldsymbol{F}_{\mathrm{v}}$ and the reference frame $\boldsymbol{F}_{\mathrm{r}}$.

For the infinitesimal rotations $\mathrm{d}\phi_{\mathrm{x}}$ about the $\boldsymbol{X}_{\mathrm{v}}^{\mathrm{v}}$ axis, we have

$$\boldsymbol{R}(X_{\mathrm{v}}^{\mathrm{v}}, \mathrm{d}\phi_{\mathrm{x}}) = \begin{bmatrix} 1 & 0 & 0 \\ 0 & \cos(\mathrm{d}\phi_{\mathrm{x}}) & -\sin(\mathrm{d}\phi_{\mathrm{x}}) \\ 0 & \sin(\mathrm{d}\phi_{\mathrm{x}}) & \cos(\mathrm{d}\phi_{\mathrm{x}}) \end{bmatrix} \approx \begin{bmatrix} 1 & 0 & 0 \\ 0 & 1 & -\mathrm{d}\phi_{\mathrm{x}} \\ 0 & \mathrm{d}\phi_{x} & 1 \end{bmatrix}.$$

We can obtain the infinitesimal rotation about the $\boldsymbol{Y}_{\mathrm{v}}^{\mathrm{v}}$-axis in a similar way. Multiplying them together and ignoring the higher order terms, we have the consecutive rotation about $\boldsymbol{X}_{\mathrm{v}}^{\mathrm{v}}$ and then $\boldsymbol{Y}_{\mathrm{v}}^{\mathrm{v}}$,

$$\boldsymbol{R}(X_{\mathrm{v}}^{\mathrm{v}}, \mathrm{d}\phi_{\mathrm{x}})\boldsymbol{R}(Y_{\mathrm{v}}^{\mathrm{v}}, \mathrm{d}\phi_{\mathrm{y}}) = \begin{bmatrix} 1 & 0 & 0 \\ 0 & 1 & -\mathrm{d}\phi_{\mathrm{x}} \\ 0 & \mathrm{d}\phi_{\mathrm{x}} & 1 \end{bmatrix} \begin{bmatrix} 1 & 0 & \mathrm{d}\theta_{\mathrm{y}} \\ 0 & 1 & 0 \\ -\mathrm{d}\theta_{\mathrm{y}} & 0 & 1 \end{bmatrix} \approx \begin{bmatrix} 1 & 0 & \mathrm{d}\theta_{\mathrm{y}} \\ 0 & 1 & -\mathrm{d}\phi_{\mathrm{x}} \\ -\mathrm{d}\theta_{\mathrm{y}} & \mathrm{d}\phi_{\mathrm{x}} & 1 \end{bmatrix}. \tag{2}$$

Observing (1) and (2), we can see that the small rotation about the $\boldsymbol{K}^{\mathrm{v}}$-axis can be decomposed into the infinitesimal rotation about the $\boldsymbol{X}_{\mathrm{v}}^{\mathrm{v}}$-axis and then the $\boldsymbol{Y}_{\mathrm{v}}^{\mathrm{v}}$-axis with $\mathrm{d}\phi_{\mathrm{x}} = k_{\mathrm{x}}\Delta\gamma$ and $\mathrm{d}\theta_{\mathrm{y}} = k_{\mathrm{y}}\Delta\gamma$, respectively. Since the $\boldsymbol{R}_{\mathrm{r}}$ and $\boldsymbol{R}_{\mathrm{n/v}}$ are always close to each other under feedback control, the rotation angle γ remains small. As a result, the rotation about the $\boldsymbol{K}^{\mathrm{v}}$-axis with angle γ can be decomposed into the rotation about the $\boldsymbol{X}_{\mathrm{v}}^{\mathrm{v}}$-axis with an angle $\phi_{\mathrm{e}} = k_{\mathrm{x}}\gamma$ and then about the $\boldsymbol{Y}_{\mathrm{v}}^{\mathrm{v}}$-axis with an angle $\theta_{\mathrm{e}} = k_{\mathrm{y}}\gamma$.

After calculating θ_{e} and ϕ_{e}, the remaining is to align the heading for $\boldsymbol{F}_{\mathrm{int}}$ and $\boldsymbol{F}_{\mathrm{r}}$ to obtain ψ_{e}. After rotating $\boldsymbol{F}_{\mathrm{v}}$ about $\boldsymbol{K}$-axis, the newly obtained $\boldsymbol{F}_{\mathrm{int}}$ has a rotation matrix with respect to the local NED frame as

$$\boldsymbol{R}_{\mathrm{n/int}} = \boldsymbol{R}_{\mathrm{n/v}}\boldsymbol{R}_{\mathrm{v/int}}.$$

Let $\boldsymbol{R}_{\mathrm{n/int}} = (\boldsymbol{X}_{\mathrm{int}}, \boldsymbol{Y}_{\mathrm{int}}, \boldsymbol{Z}_{\mathrm{int}})^{\mathrm{T}}$, ψ_{e} between the $\boldsymbol{X}_{\mathrm{int}}$ and $\boldsymbol{X}_{\mathrm{r}}$ can be computed as

$$\psi_e = \mathrm{atan2}((\boldsymbol{X}_{\mathrm{int}} \times \boldsymbol{X}_{\mathrm{r}}) \cdot \boldsymbol{Z}_{\mathrm{r}}, \boldsymbol{X}_{\mathrm{int}}\boldsymbol{X}_{\mathrm{r}}).$$

Then the angle error $\boldsymbol{e}_{\mathrm{angle}} = (\phi_{\mathrm{e}}, \theta_{\mathrm{e}}, \psi_{\mathrm{e}})^{\mathrm{T}}$ is obtained. Next, the linear quadratic regulator (LQR) controllers are designed for the three angle channels specifically. The controller design for the three angle channels are similar and for simplicity, only the pitch channel design is introduced here. By ignoring the aerodynamic force in the VTOL mode and denoting the state to be $\boldsymbol{x} = [\theta_{\mathrm{e}} \quad p \quad \int_{(\theta_{\mathrm{e}})}]^{\mathrm{T}}$, where p is the angular velocity around $\boldsymbol{Y}_{\mathrm{v}}$-axis and $\int_{(\theta_{\mathrm{e}})} = \int \theta_{\mathrm{e}}\mathrm{d}t$, the state space equation for the pitch channel is

$$\frac{\mathrm{d}}{\mathrm{d}t} \begin{bmatrix} \theta_{\mathrm{e}} \\ p \\ \int_{(\theta_{\mathrm{e}})} \end{bmatrix} = \begin{bmatrix} 0 & 1 & 0 \\ 0 & 0 & 0 \\ 1 & 0 & 0 \end{bmatrix} \begin{bmatrix} \theta_{\mathrm{e}} \\ p \\ \int_{(\theta_{\mathrm{e}})} \end{bmatrix} + \begin{bmatrix} 0 \\ 1 \\ 0 \end{bmatrix} u,$$

where u is the virtual angular acceleration input. Following the LQR controller design, $u = \boldsymbol{F}\boldsymbol{x}$ where $\boldsymbol{F}$ is designed such that the cost function

$$J = \int \boldsymbol{x}^{\mathrm{T}}\boldsymbol{Q}\boldsymbol{x} + u\boldsymbol{R}u$$

is minimized where $\boldsymbol{Q}$ and $\boldsymbol{R}$ are weighting matrix for the state and input. Then as in [11], the desired angular acceleration is mapped to desired titling angle of the vectoring thrust in pitch direction θ_{tilt} following the relationship

$$u = T\sin(\theta_{\mathrm{tilt}})L_{\mathrm{m}}/I_{\mathrm{y}}, \tag{3}$$

where T is the motor thrust, whose value is generated by the outer loop, L_{m} is the distance between the motor to the center of gravity (CG) and I_{y} is the moment of inertia of the U-Lion in pitch direction. Since the servo is chosen with sufficiently fast speed response, the dynamics of the titling is ignored and the desired tilting angle is linearly mapped to the servo input. The control law design of the other two channels are similar to this but with different actuation mappings.

The rotation matrix based RAG and the subsequent LQR controller work well in arbitrary orientation. As a result, the VTOL control has a wide range of flight envelope and this control architecture can be also applied to transition control.

3.2 Cruise mode

In the cruise mode, the attitude measurement and reference are all converted into Euler angles in the $\boldsymbol{F}_{\mathrm{c}}$ frame. Similar to the VTOL control, an LQR controller is applied for the angle control layer to generate the desired angular acceleration. As shown in [11], torque generated by each control surface is

$$M(\delta_{\mathrm{fin}}) = \pi\delta_{\mathrm{fin}}\rho V_{\mathrm{air}}^2 S_{\mathrm{fin}}l_{\mathrm{fin}}, \tag{4}$$

where $M(\delta_{\mathrm{fin}})$ is the torque generated by the control fin, δ_{fin} is the deflection angle of the control fin, ρ is the air density, V_{air} is the airspeed, S_{fin} is the control surface area and l_{fin} is the distance from the control surface to the CG. Following the above-mentioned relation, the desired angular acceleration is mapped to the control surface deflection angles. Thus the cruise flight mode inner loop control is completed.

3.3 Transition mode

The transition mode serves as an important bridge between the VTOL mode and the cruise mode. Due to the high AOA situation faced in the transition process, the aerodynamic forces and moments of U-Lion is difficult to analysis. As a result, the transition process is difficult to automate. In the initial stage of U-Lion development, we propose a practical method to automate the transition process with the following steps:

1. Design an acro controller for attitude rates only.

2. Performing manual flight for VTOL to cruise (forward) and cruise to VTOL (backward) transitions.

3. Fit the pitch and throttle data during manual transition into rotation matrix and throttle input trajectories.

4. Design feedback controller for tracking the trajectories.

Step 1: Denote the angular velocity to be $\boldsymbol{\omega}$, the moment of inertia of U-Lion to be $\boldsymbol{I}$, then based on D'Alembert-Lagrange equation, the compact form of moment equation in body frame can be formulated as

$$\boldsymbol{I}\dot{\boldsymbol{\omega}} = -\boldsymbol{\omega} \times (\boldsymbol{I}\boldsymbol{\omega}) + \boldsymbol{M}_{\mathrm{aero}} + \boldsymbol{M}_{\mathrm{vectorT}} + \boldsymbol{M}_{\mathrm{surface}} + \boldsymbol{M}_{\mathrm{d}},$$

where $\boldsymbol{M}_{\mathrm{vectorT}}$ is the torque provided by the vectoring thrust, $\boldsymbol{M}_{\mathrm{aero}}$ is the aerodynamic torque, $\boldsymbol{M}_{\mathrm{surface}}$ is the torque provide by the control surfaces of U-Lion and $\boldsymbol{M}_{\mathrm{d}}$ is disturbance and model uncertainties. Since the aerodynamic torque is difficult to estimate in the fast transition with high AOA situation, this term is also treated as disturbance. Denote the $\boldsymbol{M}_{\mathrm{u}}$ as the control input where $\boldsymbol{M}_{\mathrm{u}} = \boldsymbol{M}_{\mathrm{vectorT}} + \boldsymbol{M}_{\mathrm{surface}}$, then the nominal dynamics is

$$\boldsymbol{I}\dot{\boldsymbol{\omega}} = -\boldsymbol{\omega} \times (\boldsymbol{I}\boldsymbol{\omega}) + \boldsymbol{M}_{\mathrm{u}}.$$
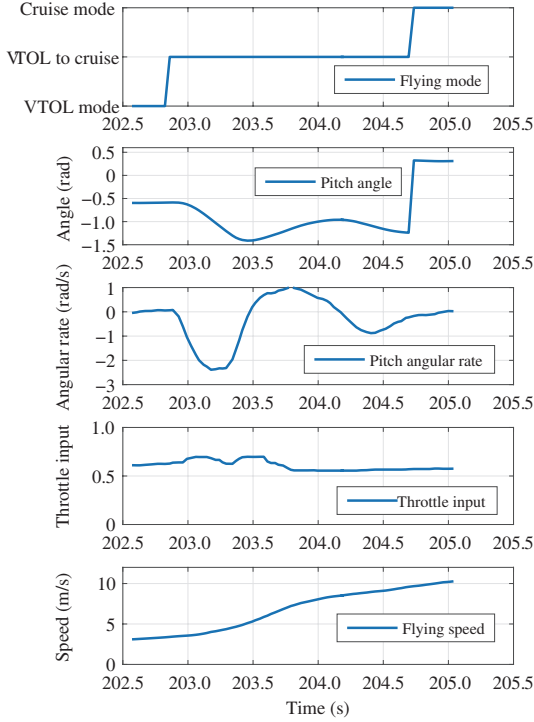
Figure 7 (Color online) Manual forward transition data.
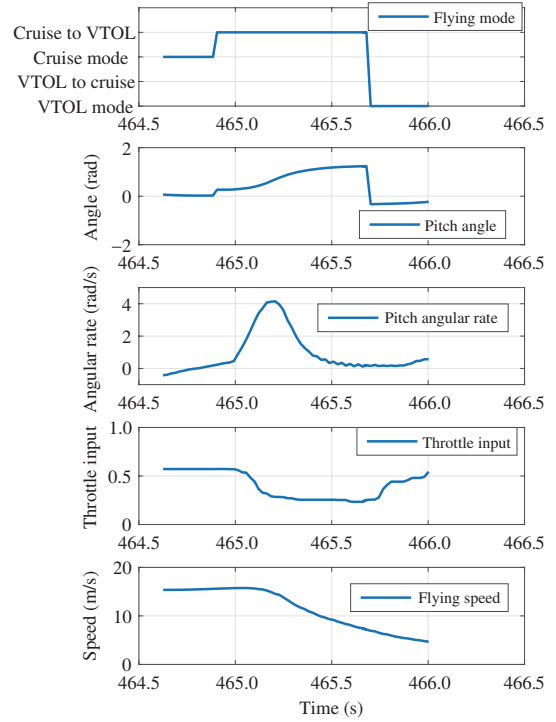
Figure 8 (Color online) Manual backward transition data.

The acro feedback controller is designed as

$$\boldsymbol{M}_{\mathrm{u}} = \boldsymbol{K}_\omega(\boldsymbol{\omega}_{\mathrm{r}} - \boldsymbol{\omega}) + \boldsymbol{\omega} \times (\boldsymbol{I}\boldsymbol{\omega}), \tag{5}$$

where the $\boldsymbol{K}_\omega$ is the feedback gain and $\boldsymbol{\omega}_{\mathrm{r}}$ is the angular rate references. The $\boldsymbol{M}_{\mathrm{u}}$ is then mapped to the vectoring thrust and different control surfaces input following the similar relationship in (3) and (4). With the acro controller designed, the attitude of U-Lion is dynamically stable with fast response which is suitable for performing manual transitions.

Step 2: We designed a manual control mode with above-mentioned three flight modes (i.e VTOL mode, cruise mode and acro mode) and a switch to trigger the switching between different modes. An experienced human pilot has performed several transitions in the manual control mode. The flight data of one forward and one backward transition is shown in Figures 7 and 8 respectively.

Step 3: From Figure 7, it can be seen that the transition started at 202.8 s with pitch angle $\theta_{\mathrm{i}}^{\mathrm{v}} = -0.5$ rad, flying speed of 3 m/s and reached an final state before switching to cruise mode with pitch angle $\theta_{\mathrm{f}}^{\mathrm{v}} = -1.35$ rad and flying speed of 9 m/s. The pitch angle changed by a angle of $\pi/2$ when flying mode switched to cruise mode due to change of frame. In the transition process, the pitch rate smoothly accelerated to -2.4 rad/s and then decelerated back to 0 rad/s afterwards. The pitch angle kept around -1.1 rad in $\boldsymbol{F}_{\mathrm{v}}$ or around $25°$ in $\boldsymbol{F}_{\mathrm{c}}$ to accelerate to the flying speed of 9 m/s before swithcing to cruise mode. The throttle input $\delta_{\mathrm{throttle}}^*$ is around 0.7 in the forward transition process.

We adopted the jerk limited trajectory generation algorithm (JLTGA) proposed in [12,13] to generate smooth trajectory for fitting the manual flight pitch angle and pitch angular rate path. The algorithm is able to generate a jerk limited trajectory for a given initial state $(\theta_{\mathrm{i}}, q_{\mathrm{i}})$ to an final state $(\theta_{\mathrm{f}}, q_{\mathrm{f}})$ with angular rate q, angular acceleration a_θ and angular jerk j_θ in a given limited range. The fitting result is shown in Figure 9 and the parameters for the trajectory generation algorithm is presented in Table 2. The backward transition manual flight data is shown in Figure 7. The analysis is similar to the forward transition and the fitting result is shown in Figure 10 . The parameters for the backward transition is also shown in Table 2.

With the JLTGA parameters obtained, during each transition, either forward or backward, the pitch angle trajectory $\theta^*(t)$ and pitch rate trajectory $q^*(t)$ could be generated. Then together with the initial
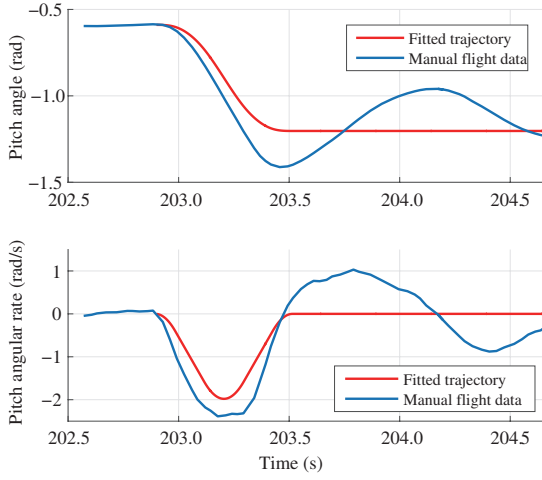
Figure 9 (Color online) Manual forward transition data.
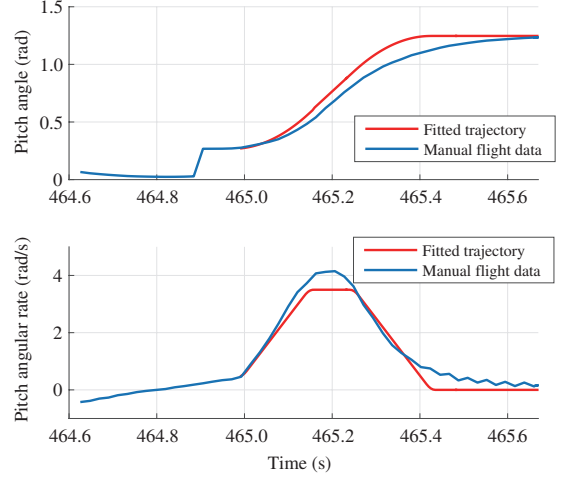
Figure 10 (Color online) Manual backward transition data.

Table 2 The parameters for the JLTGA

	Forward transition	Backward transition
Maximum angular rate	2 rad/s	3.5 rad/s
Maximum angular acceleration	9 rad/s^2	20 rad/s^2
Maximum angular jerk	100 rad/s^3	1000 rad/s^3
Targeting pitch angle (in $\boldsymbol{F}_\mathrm{c}$)	25°	90°

yaw angle reference when transition starts and zero roll angle reference, the rotation matrix trajectory $\boldsymbol{R}^*_\mathrm{tran}(t)$ and angular rate trajectory $\boldsymbol{\omega}^*(t) = (0, q^*(t), 0)^\mathrm{T}$ could be generated for the transition process.

Step 4: At a given time in the transition process, the rotation matrix reference could be obtained in above-mentioned method. Then applying the same RAG as in the VTOL mode, we could obtain the angle error $\boldsymbol{e}_\mathrm{angle}(t) = (\phi_\mathrm{e}(t), \theta_\mathrm{e}(t), \psi_\mathrm{e}(t))^\mathrm{T}$. Next, a feedback controller is designed to obtain the angular rate reference with

$$\boldsymbol{\omega}_\mathrm{r}(t) = \boldsymbol{K}_\mathrm{p,tran}\boldsymbol{e}_\mathrm{angle}(t) + \boldsymbol{\omega}^*(t),$$

where $\boldsymbol{K}_\mathrm{p,tran}$ is the feedback gain for the angle error. Finally, the angular rate reference is passed to the acro controller in (5) to complete the transition attitude controller. The throttle channel is designed as

$$\delta_r = K_\mathrm{airspeed}(V_\mathrm{airspeed,ref} - V_\mathrm{airspeed}) + \delta^*_\mathrm{throttle},$$

where K_airspeed is the feedback gain, $V_\mathrm{airspeed,ref}$ is the targeting airspeed and V_airspeed is the current flying airspeed. When the flying speed and attitude falls in the stabilizing criteria of the targeting flying mode, the control mode is switched afterwards.

4 Outer loop control system design

In this manuscript, the autonomous flight mission of U-Lion refers to taking off and landing in VTOL mode while traversing waypoints in cruise mode. To fulfill a flight mission with two flying modes, the outer loop is decomposed into three layers, the trajectory generation algorithm (TGA) layer, the outer loop control logic layer, and the outer loop control algorithm layer, as shown in Figure 11. The TGA layer generates the trajectory reference based on the mission requirements. Then the outer loop control logic layer determines the operation mode and triggers mode switching when required. The outer loop control algorithm layer selects the corresponding outer loop control algorithm and follows the trajectory generated in TGA layer.

4.1 TGA layer

Similar to [7], a nonlinear L1 guidance algorithm described in [14] is utilized to generate the trajectory reference for autonomous flight of U-Lion. The L1 guidance algorithm is one of the most commonly used
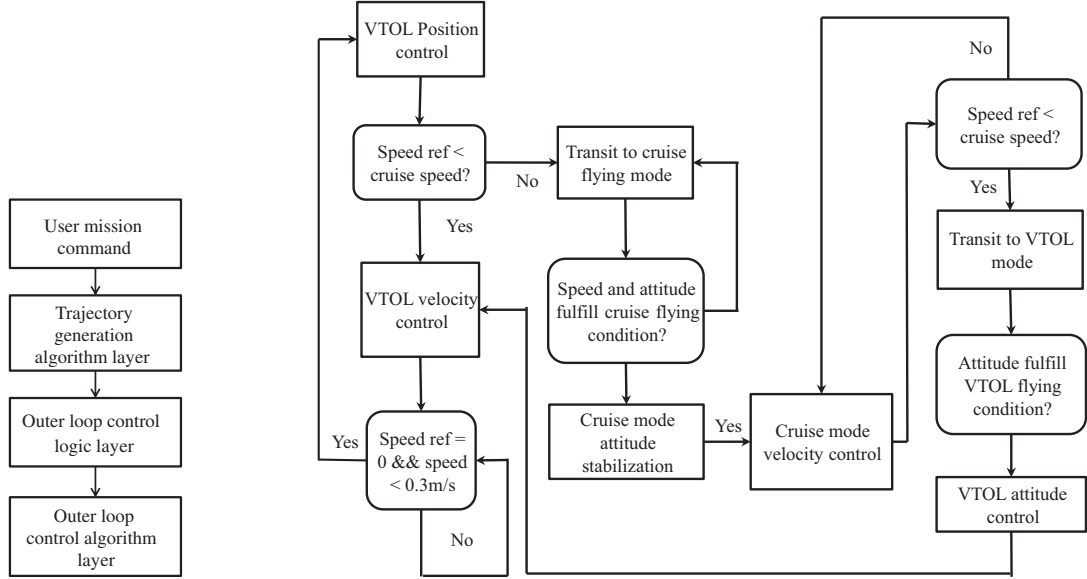
Figure 11 Outer loop overall structure.

Figure 12 The autonomous control logic.

trajectory generation algorithms for fixed wing UAV. The main algorithm for L1 guidance is to generate a commanding centripetal acceleration for a given velocity to track the given path:

$$a_{s_{cmd}} = 2\frac{V_{airspeed}^2}{L_1}\sin\alpha,$$

where L_1 is the distance of the reference point on the desired path forward of the vehicle, and α is the angle between the velocity vector and vector from vehicle position to the reference point. The L1 guidance algorithm focuses more on the velocity direction for fixed wing UAVs while the speed reference is normally fixed. However, since the U-Lion is equipped with VTOL capability, the L1 guidance algorithm is modified so that the reference speed is also planned. For a certain mission, based on the distance between the target position to the UAV, the speed reference will be generated using the same JLTGA introduced in previous text. Then U-Lion will accelerate to a certain speed to approach the target position and could stop at the target position in the VTOL mode following the speed reference. In altitude direction, the JLTGA is also utilized to generate the altitude position and velocity references for a given mission.

4.2 Control logic layer

The control logic for U-Lion autonomous flight is shown in Figure 12. The control logic starts with VTOL position control. Based on the TGA, if the speed reference is not zero but less than the cruise speed of U-Lion, the VTOL velocity control loop will be turned on. The velocity reference is derived from the speed reference and the lateral acceleration reference from the modified L1 TGA, as can be seen in Figure 13.

If the speed reference is greater or equal to the nominal cruise speed of the U-Lion, the transition from VTOL to cruise mode will be triggered. In the transition process, the transition inner loop control will be activated to push the head of U-Lion down and accelerate as described in Subsection 3.3. When the pitch angle and the speed of U-Lion fall in the controllable region of cruise mode, the control mode will be switched to cruise mode.

Finally, when approaching the target waypoint that requires U-Lion to hover, based on the TGA, the speed reference will decrease to 0. The transition control will be triggered again to pull U-Lion head up for VTOL flight. After the attitude of U-Lion falls in the controllable region of VTOL attitude control, the VTOL attitude control will be activated. After that, the velocity control will be triggered to decelerate U-Lion for a complete stop with VTOL position control.

Figure 13 The outer loop control structure.
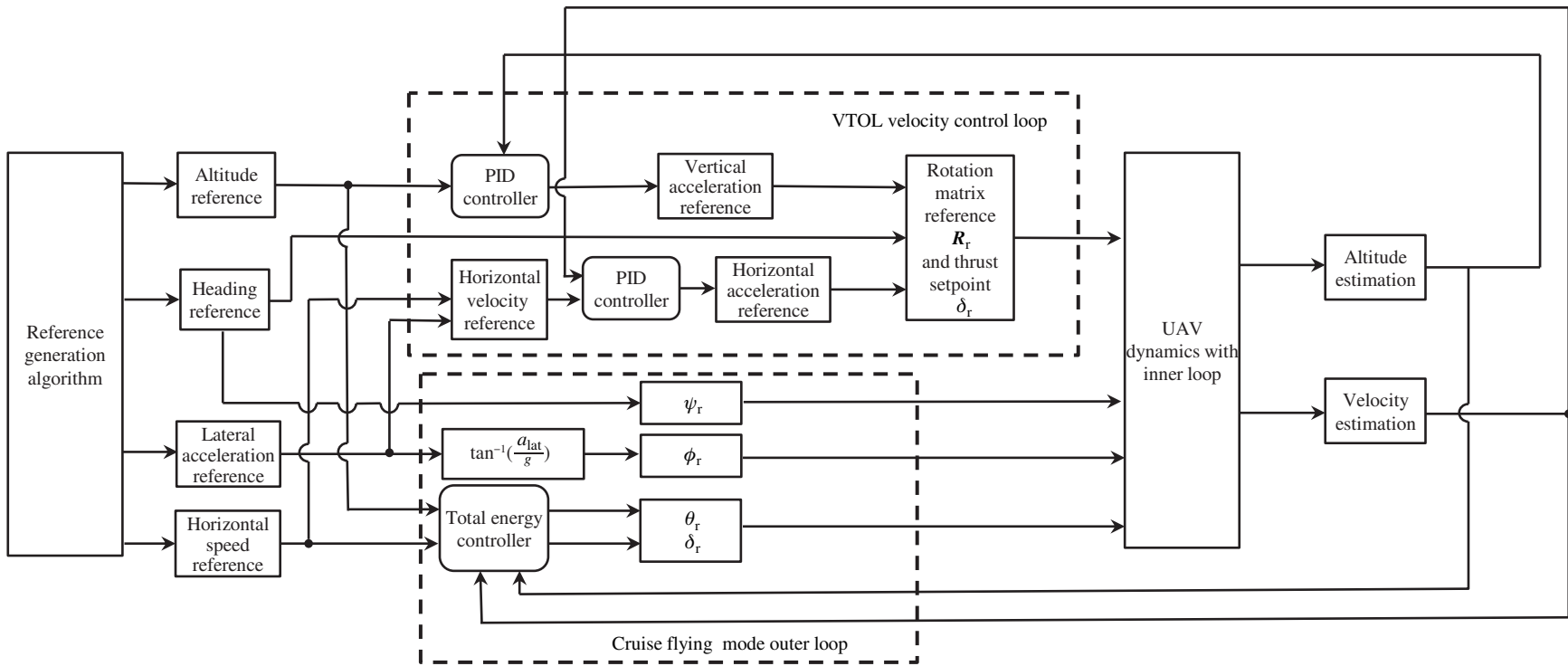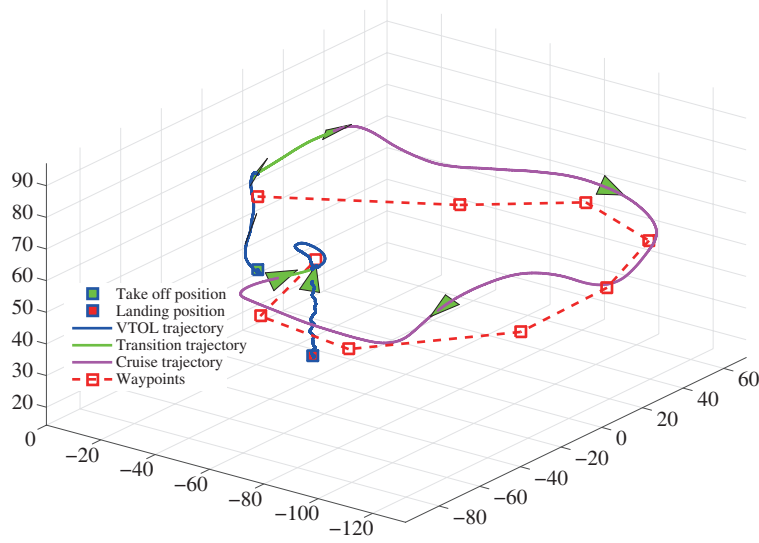
Figure 14   (Color online) The position result for the fly test.

4.3   Control algorithm layer

As shown in Figure 13, for the VTOL velocity control loop, the horizontal velocity reference is passed into a PID controller to generate the horizontal acceleration reference. The altitude PID controller will generate a vertical acceleration reference in VTOL mode. Then the direction of the reference $\boldsymbol{Z}_{\mathrm{r}}$-axis and the magnitude of the thrust in VTOL mode can be generated from the acceleration references. Together with the heading reference from the TGA, the inner loop references are generated. The transition from the velocity control to the position control happens when the speed reference is zero and the speed measurement is less than a threshold. When position control is triggered, the current position of U-Lion is set to be the position reference, and the velocity reference will be generated through a proportional controller and then passed to the VTOL velocity control loop.

In cruise mode, since the TGA generates the lateral acceleration reference a_{lat}, the roll angle reference in $\boldsymbol{F}_{\mathrm{c}}$ frame can be directly obtained as

$$\phi_{\mathrm{r}} = \tan^{-1}\left(\frac{a_{\mathrm{lat}}}{\mathrm{g}}\right).$$

The pitch reference and the thrust setpoint is obtained from a total energy controller (TEC) proposed in [15]. The TEC is widely used for fixed wing autonomous height and speed control. The proposed energy rate and energy distribution rate decouple the cross coupling dynamics for the fixed wing height and speed control. Then together with the heading reference from TGA, the cruise mode inner loop references are obtained.

5   Experimental flight test results

We conducted an outdoor flight test to verify the platform design and the effectiveness of the proposed control algorithm. The flight includes an autonomous take-off, bi-direction transitions, cruise flight following waypoints, and autonomous landing. The 3-D position response of U-Lion during the flight is shown in Figure 14. The green triangles represent the position and the orientation of U-Lion during the flight, the blue trajectories are the VTOL trajectories, green trajectories are the transition trajectories, the magenta color trajectory is the cruise flying trajectory. The flying mode, altitude response and speed during the flight are presented in Figure 15. The roll angle, pitch angle and flight path angle data is shown in Figure 16.

As shown in Figure 14, U-Lion started at the green square position in VTOL mode and took off to a height of 30 m. After hovering for around 10 s, it started to transit for traversing waypoints. During the
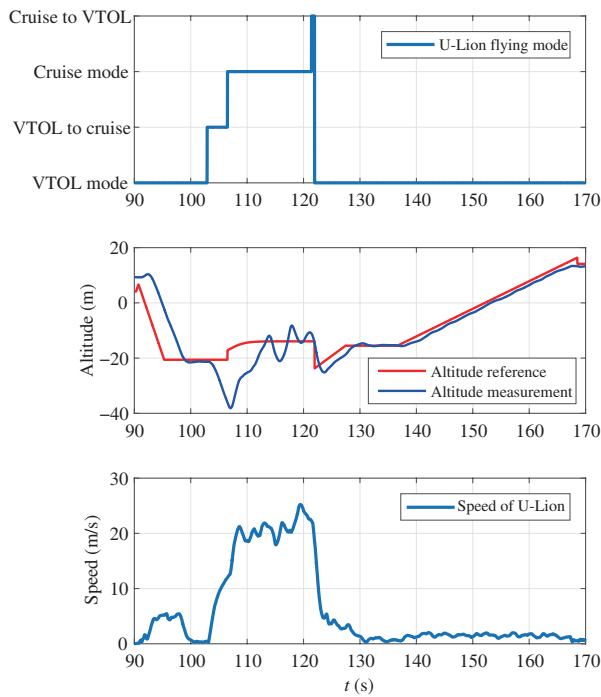
Figure 15 (Color online) Flight data.
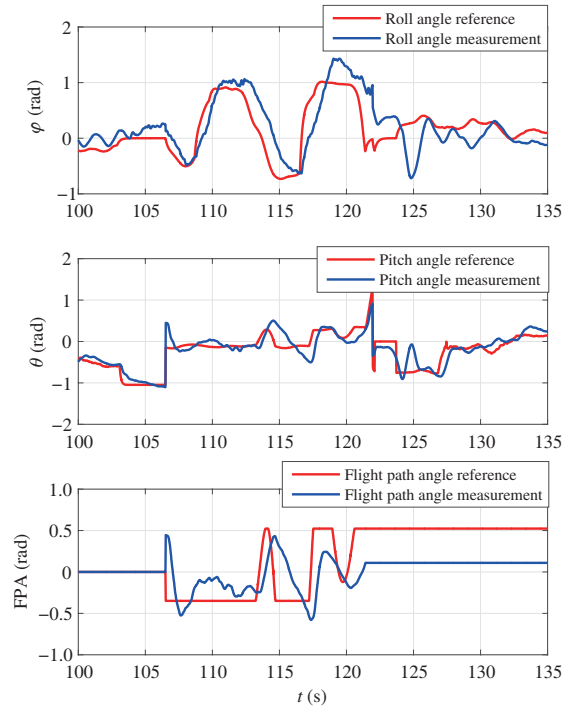
Figure 16 (Color online) Flight angle data.
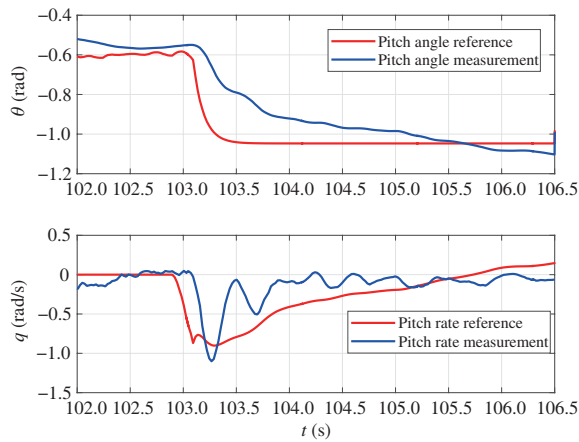
Figure 17 (Color online) Forward transition pitch angle data.
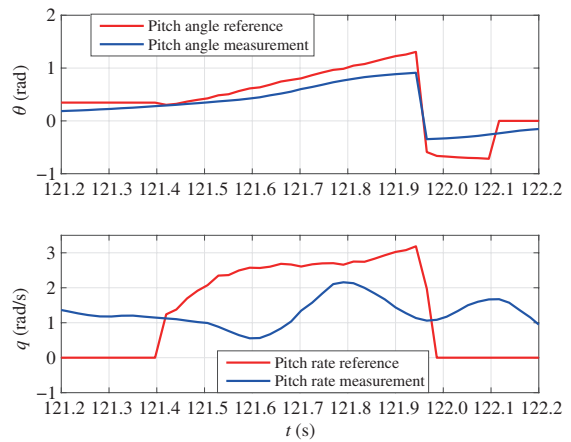
Figure 18 (Color online) Backward transition pitch angle data.

forward transition, U-Lion started with pitching down and accelerating following the transition controller described in Subsection 3.3. When the UAV speed reached 12 m/s, the flying mode was switched to cruise mode subsequently. Then U-Lion started to track the pre-defined waypoints in cruise flying mode. When U-Lion reached the last waypoint, it transited back to VTOL mode for a complete stop followed by autonomous landing to the red square position.

From the first plot of Figure 15, it can be seen that the forward transition happened at time 103 s and last around 3.5 s. The backward transition started at 121.4 s and took around 1 s. As shown in Figures 17 and 18, the pitch angle references follow the trajectory generation algorithm proposed in Subsection 3.3. The rate reference follows the transition logic proposed and led U-Lion for smooth transitions. The successful autonomous transition flight demonstrates the effectiveness of the proposed transition control law.

As shown in the second plot in Figure 15, the height control performance is satisfactory in the VTOL mode with maximum height control error less than 1 m. While the height control performance in cruise

mode is not as good as the VTOL mode. There is a bit of oscillation in height and the maximum error is around 5 m. The height control performance in cruise mode is determined by the flight path angle (FPA) control performance as shown in the third plot in Figure 16. The FPA control performance was constrained by the model accuracy in the initial stage and will be further improved in the future research.

Due to the space limitation of flying area, the turning radius between subsequent waypoints was too small for U-Lion to track. Besides, since all the waypoint line segments were too short and the L1 guidance algorithm had to continuously switch target point on different line segments before the tracking on one line segment converged. As a result, the roll angle reference during cruise flight kept alternating between maximum allowed values as shown in the first plot of Figure 16. Nevertheless, the tracking performance of roll angle was satisfactory and resulted in acceptable tracking performance of waypoints for cruising speed of 20 m/s. The next focus of our research is to develop the detailed modelling for U-Lion and improve the flight control performance.

Overall, the flight results demonstrated the principle of the hybrid UAV which will take off and land vertically while traversing the waypoints in considerable cruise speed automatically.

6 Conclusion

We have presented in this paper an autonomous hybrid tail-sitter UAV code-named U-Lion. Compared to the earlier platforms developed, the present design is of lighter weight, more compact size and more efficient aerodynamic structure. The direct drive vectored thrust ensures sufficient controllability in VTOL mode and transitions. Rotation matrix based VTOL/transition inner loop control and Euler angle based cruise inner loop control algorithms are developed and realized with a complete framework for the autonomous flight including bi-directional transitions. The overall design has been successfully tested in actual flight experiments. Our future research focus is to further improve the platform structure and control performance, as well as to integrate the vision-based target detection and tracking system of [16] to carry out some real applications.

Conflict of interest The authors declare that they have no conflict of interest.

Supporting information The supporting information is available online at info.scichina.com and link.springer.com. The supporting materials are published as submitted, without typesetting or editing. The responsibility for scientific accuracy and content remains entirely with the authors.

References

1 Bapst R, Ritz R, Meier L, et al. Design and implementation of an unmanned tail-sitter. In: Proceedings of IEEE/RSJ International Conference on Intelligent Robots and Systems (IROS), Hamburg, 2015. 1885–1890
2 Oosedo A, Abiko S, Konno A, et al. Development of a quad rotor tail-sitter vtol uav without control surfaces and experimental verification. In: Proceedings of IEEE International Conference on Robotics and Automation (ICRA), Karlsruhe, 2013. 317–322
3 Ang K Y Z, Cui J Q, Pang T, et al. Design and implementation of a thrust-vectored unmanned tail-sitter with reconfigurable wings. Unmanned Syst, 2015, 3: 143–162
4 Selig M S, Guglielmo J J, Broeren A P, et al. Summary of Low-Speed Airfoil Data. Virginia Beach: SoarTech Publications, 1995
5 Anderson Jr J D. Fundamentals of Aerodynamics. 5th ed. Boston: McGraw-Hill, 2010
6 Meier L, Honegger D, Pollefeys M. PX4: a node-based multithreaded open source robotics framework for deeply embedded platforms. In: Proceedings of IEEE International Conference on Robotics and Automation (ICRA), Seattle, 2015. 6235–6240
7 Wang K L, Ke Y J, Chen B M. Development of fully autonomous hybrid UAV U-Lion with vertical and cruise flying capabilities. In: Proceedings of IEEE International Conference on Advanced Intelligent Mechatronics, Banff, 2016
8 Brescianini D, Hehn M, D'Andrea R. Nonlinear quadrocopter attitude control. Technical Report. Department of Mechanical and Process Engineering, ETHZ. 2013
9 Faessler M, Fontana F, Forster C, et al. Automatic re-initialization and failure recovery for aggressive flight with a monocular vision-based quadrotor. In: Proceedings of IEEE International Conference on Robotics and Automation (ICRA), Seattle, 2015. 1722–1729

10 Mayhew C G, Sanfelice R G, Teel A R. Quaternion-based hybrid control for robust global attitude tracking. IEEE Trans Automat Control, 2011, 56: 2555–2566

11 Ke Y J, Wang K L, Chen B M. A preliminary modeling and control framework for a hybrid UAV J-Lion. In: Proceedings of International Micro Air Vehicle Conference, Beijing, 2016

12 Lai S P, Wang K L, Qin H L, et al. A robust online path planning approach in cluttered environments for micro rotorcraft drones. Control Theory Technol, 2016, 14: 83–96

13 Phang S K, Lai S P, Wang F, et al. Systems design and implementation with jerk-optimized trajectory generation for UAV calligraphy. Mechatronics, 2015, 30: 65–75

14 Park S, Deyst J, How J. A new nonlinear guidance logic for trajectory tracking. In: Proceedings of AIAA Guidance, Navigation, and Control Conference and Exhibit, 2004. AIAA 2004-2900

15 Lambregts A A. US Patent, 6062513, 2000

16 Lin F, Lum K Y, Chen B M, et al. Development of a vision-based ground target detection and tracking system for a small unmanned helicopter. Sci China Ser F-Inf Sci, 2009, 52: 2201–2215